Pipeline detection system from acoustic images utilizing CA-CFAR

Sebastián A. Villar (1), Gerardo G. Acosta (1)(2), André Sousa Senna (2), and Alejandro Rozenfeld (1)(2),

(1) INTELYMEC Group, CIFICEN-CONICET, Faculty of Engineering, National University of Buenos Aires Province Center, Argentina.
(2) GEE – Physics Dept., University of the Balearic Islands, Spain.

E-mail: ggacosta@fio.unicen.edu.ar

Abstract- **The Side Scan Sonars (SSS) are one of the most utilized devices to obtain acoustic images of the seafloor. To face an application of preventive maintenance of the underwater infrastructure, it was necessary to realize a detection system and pipeline exploration in automated form. The current techniques of acoustic images processing of SSS consume a great quantity of time and computational resources. Thus, an efficient system of pipeline detection is presented utilizing techniques of Cell-Averaging with Constant False Alarm Rate (CA-CFAR). These proposals were contrasted experimentally on images obtained from wet tests in Salvador da Bahia with promising results.**

Index Terms- **CA-CFAR, side scan sonar, images processing.**

I. Introduction

The majority of the underwater tasks, such as the pipeline inspection and maintenance, resources search, mine detection, or debris recognition, are intended to be developed in an automatic way by using autonomous underwater vehicles (AUV). In the particular case of pipeline maintenance, it is necessary to detect and then track them, obtaining as much information as possible about their situation (on the sea floor, buried, with corrosion, covered with sediments, among others). An AUV is able to perform a precise and detailed observation task regarding aspects of interest such as damage evaluation, harmful waste, hooked anchors and others. The technology for the complete automation of underwater tasks has evolved in the last years due to the improvements with respect to (1) AUVs technology, (2) new perception devices, and (3) new techniques of acoustic images processing for objectives detection and classification.

As regards point (1), the AUVs have been experiencing a sustained grade of advance, in relation to their technology, the algorithms for on board signals processing, and their control approaches [1] - [5].

In reference to point (2), one of the most utilized devices to obtain acoustic images are SSS. They represent an efficient tool to ensonify objects on the seafloor [3]. A conventional SSS provide lines of acoustic pulses that vary from 200 to 2000 samples. This value has relation with the range in meters which is acquired from the sea floor, which constitutes a trade-off between the range covered on the one hand, and the time and processing resources to analyze that amount of data, on the other hand. Thus, the more meters covered, the greater the resources consumed. The capacity of high resolution acoustic images processing within the AUV is a fundamental issue to give the vehicle decision autonomy. While the sailing, orientation and AUV control technologies, as well as the perception devices have become mature enough for the vehicle autonomy; it is not the same with on-line acoustic image processing. Many approaches are currently available. They much vary in their speed, efficiency, CPU resources needed, precision and robustness [6] - [18].

A group of objective detection techniques widely used in the technology of RADAR (*RAdio Detection And Ranging*) is known as CFAR, *Constant False Alarm Rate* [19]. This group of techniques maintains a Constant False Alarm Rate, where interference energy must be estimated with the data. Thus, the detection threshold is adjusted to maintain a probability of expected False Alarm (P_{fa}). If the interference energy and the threshold are estimated with the average of the values of the adjacent cells, this approximation is denominated CA-CFAR (*Cell Averaging-Constant False Alarm Rate*) [20]. Since the technology of SONAR (*SOund NAvigation And Ranging*) is close to the RADAR technology [21], the proposal of this work is to migrate the mentioned RADAR detection technique to the objects detection in the seabed, such as pipeline, from acoustic images.

Hence, the objectives explored in this article concentrate in the acoustic images processing obtained by SSS devices and in allowing adequate pipeline detection on the sea floor. Also, they focus in reducing time and computational resources in such a way that this task could be solved in efficient time. Specifically, the CA-CFAR technique is presented and it is demonstrated that the automatic pipeline detection with it is possible and efficient.

This work is organized in the following way: Section 2 starts by showing the acoustic input data formation. Then, in Section 3 an automatic processing chain is presented for a pipeline detection system, describing each process that make up the chain. Section 4 focuses on the basic concepts of the detection theory, with an introduction of the technique CA-CFAR. In Section 5, the experimental result, analyses and comparisons are shown. Finally, Section 6 presents the conclusions obtained in the work.

978-0-933957-40-4 ©2013 MTS

II. FORMING ACOUSTIC IMAGES FROM A SSS

The SSS are the principal visualization tool which provides acoustic images of the sea floor [3]. The SSS and the Synthetic Aperture Sonars (SAS) are two types of side scan sonars. The SSS represents one of the most popular sonar, because they have been tested in deep waters with very satisfactory results [22] - [26], even though lately a more intensive use of SAS is appreciated due to the high quality of the acquired data [27] - [31]. It is also described the use of the *multibeam echo sounders* – MBE to explore in detail the sea floor in [22] y [32] - [34].

The SSS is formed by a group of hydrophones which are mounted in the sides of the vehicle. In each data acquisition cycle, these hydrophones scan sideways and downward, constituting a vertical plane which advances in the direction of the vehicle orientation, called *along-track*. Fig. 1 shows an idealized representation of the operation of a SSS mounted on an AUV.

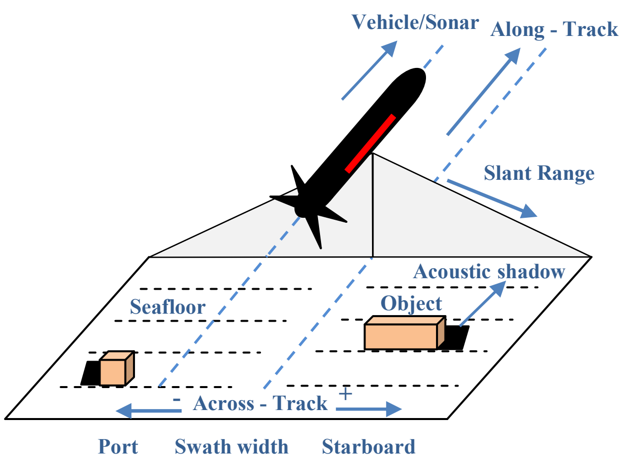

Figure 1: Operation of the side scan sonar on AUV.

The transducers on both sides of the sonar send oblique acoustic signals, in the shape of a fan, in perpendicular planes to the AUV trajectory (*across-track*). These acoustic pulses normally oscillate between 100 and 500 kHz. The port side (left) and starboard (right) of the images are scanned separately. The acoustic pulses travel along the water column, hit the seafloor and the echo is returned to the reception sensor from where its amplitude is quantified. This amplitude depends on the angle of incidence of pulses and also on the material of the seafloor.

The echoes coming directly from the seafloor, also called backscattering, constitute the signal of analysis. The returns to the sonar by means of multiple bounces of the seafloor or the sea surface constitute the reverberation or not desired echoes. The regions under the sonar (*nadir*) and above the sonar (*zenith*) correspond to points of low and high reflection of the surface of the seafloor and the surface of the sea, respectively.

The data acquired are projected on a line traced along the seafloor. This scanning line is known as *swath*. These acoustic data which contain this exploration line represent an observation of the reflected intensity depending on the range and the angle. The movement of the vehicle provides a second dimension, perpendicular to the first. If the vehicle is moving in a straight line at a steady speed, the scanning of the parallel lines will build an acoustic image of the seafloor. If the scanning is carried out on both sides of the platform, an image is acquired duplicating the coverage rate [4].

III. PIPELINE DETECTION SYSTEM

Each swath acquired by the SSS is introduced in an *automatic processing chain*. This processing chain is formed by a set of processes. The input to one process represents the output of the previous process. Fig. 2 shows a block diagram of a simple processing chain utilized in a detection system. As it can be seen, the input is an acoustic swath provided by the SSS; and the output consists of a list of geo-referenced (NED) coordinates of the pipeline position.

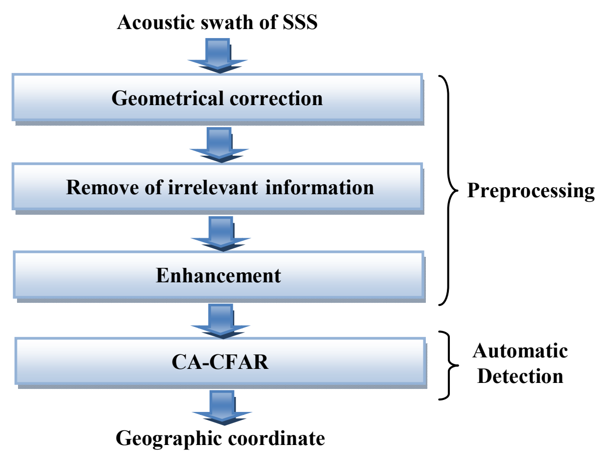

Figure 2: Automatic processing chain for the pipeline detection system

As it appears from the observation of Fig. 2, before applying the ***automatic detection*** process (see section 4), the acoustic data are pre-processed to improve incoming data.

The first process consists in the ***geometrical correction*** of the distortion by inclination. The SSS acoustic images are prone to have numerous perturbations, geometrical and natural, which interfere in the detection process [4], [35] y [36]. For instance, the distortion by AUV's attitude changes corresponds affects the relative position of features in the acoustic image and its true location in the sea floor. In this case study, the relative orientation of the pipeline and its real position is a fundamental system requirement. This distortion represents a process of corrections which have two adjustments, one on the *across-track* direction and the other on the *along-track* direction. To carry out this correction, a simple trigonometric relation is applied [3] utilizing navigating data such as altitude, the slant-range and the angle of incidence, directly proportional to the *ground-range*. Also, the following strong suppositions must be assumed [37]: 1) The seafloor is plane and horizontal; 2) The acoustic pulse is propagated through the water at a constant speed; 3) The roll angle of the vehicle is null, because it does not contribute to the geometric distortions; 4) The vehicle is immobile from the moment the acoustic pulse is shot until the return of the maximum range is received.

Then, an acoustic image is defined as a function of two dimensions of discrete finite values $f[n,m]$, where $[n,m]$ represent the spatial coordinates. The amplitude in any pair of coordinates $[n,m]$ is called intensity of the monochromatic image [9]. This intensity or backscatter force of the sea floor is defined as $b(x,y)$, where x and y are part of a system of rectangular coordinates (x,y,z) defined in the sea floor. This coordinates system is aligned to the direction y with the trajectory of the vehicle, i.e. to the *along-track* direction; and x is aligned with the *across-track* direction. Thus, if $f[n,m]$ is the original image and $h[m]$ the altitude of water column in pixels for the line m, it can be stated that the corrected image $\boldsymbol{g}$ can be obtained as follows:

$$g[l,m] = f[n,m] \; such\ that \;\; n = \sqrt{h^2[m] + l^2} \quad (1)$$

For $\boldsymbol{l} = \mathbf{0}, \pm\mathbf{1}, \pm\mathbf{2}, \dots, \pm(\boldsymbol{N_l} - \mathbf{1})$ and $\mathbf{m} = \mathbf{0}, \mathbf{1}, \dots, \mathbf{N_m} - \mathbf{1}$, where $\boldsymbol{N_m}$ is the number of horizontal lines in the corrected image and $\boldsymbol{N_l}$ is the number of pixels of line per side. The value of $\boldsymbol{n}$ which corresponds to $\boldsymbol{l}$ generates a noninteger value, and then an interpolation between the adjacent pixels must be carried out.

The following process consists in the ***elimination of irrelevant information***. The acoustic images contain, in the center, a black track denominated a *blind spot*. This region under the sonar (*nadir*) is inherent to this type of images. This irrelevant information must be substituted because it generates a brusque variation of shades, dark to light, generating false detections. For that, in each acoustic line, the greatest shadow limit is detected on both port side and starboard side. Also, it is positioned in the center of the sonar line and it is traversed both on the right and on the left until the greatest brusque variation of shades is found. Finally, a threshold value is computed, which represents the brightness of the blind zone limit. Thus, the limits for each acoustic line are obtained, within which no processing will be carried out.

Another issue is the ***image enhancement***, about which extensive literature exists [9], [10] y [35]. While most of the traditional techniques of image processing are not adequate to the improving of the acoustic image, it must be yet determined if it is really useful the application of this process in these acoustic images.

IV. Automatic

The problem of detection is summed up in analyzing each sample with the objective of detecting the presence or absence of an objective. Richards [20] defined two hypotheses for this analysis: 1) *the sample is the result of interference* (H_0) and 2) *the sample is the result of a combination between interference and echoes of an objective* (H_1). Consequently, the detection consists in examining each sample and selecting one of these hypotheses as the best. If the hypothesis H_0 is the most appropriate, the detection system declares that the objective is not present. On the other hand, if the hypothesis H_1 is the most appropriate, the detection system declares that the objective is present. Because of the signals are described statistically, the decision between these two hypotheses represents an application of the statistics decision theory [38].

In the particular case of acoustic images, it should be considered that the objects on the sea floor are usually more reflective than the surrounding sediment. For this reason, one of the detection alternatives is centered in finding the maximum intensities or *acoustic highlight*, which varies considerably according to the sonar relative orientation with the object. In fact it can even fall below the detection threshold causing the object to be invisible.

On the other hand, an additional relevant characteristic of this type of acoustic images is that the objects which protrude above the seafloor generate *shadows*. That is to say, areas where the echo intensity is frequently lower than the level coming from the seafloor. The shadow longitude depends on the vertical height of the object. Thus, another detection alternative is resorting to these shadows.

Due to the acquisition is carried out from a moving vehicle, the sonar geometry as regards the objective is variable; a shadow can be present even when the acoustic projection is not. Thus, it would be desired to combine both detection approximations, as it is proposed in this work.

The following Fig. 3 shows a generic architecture of the process CA-CFAR [39] y [40]. CA-CFAR is an adaptive technique which estimates the detection threshold (T) based in the test cell surroundings (x_i) the threshold multiplier (α). In this way, it has into account both the *acoustic highlight* and the *shadow* that the objects generate. The technique assigns strong return values when the acoustic highlight is proportional to the area of the object frontal part, and shadow values when it is proportional to the longitude of the shadow behind the object. These abrupt variations between a highlight range and acoustic shadow generate the objective detection possibility. The technique CA-CFAR maintains constant false alarm rate (P_{fa}), which is utilized to calculate the threshold multiplier (α). The detection threshold (T) is adjusted to maintain a desired probability of false alarm (P_{fa}). The current test cell (x_i) is compared to the detection threshold. If the test cell value exceeds the threshold, the process declares that the objective is present. Then, the following cell is proved, applying the process again.

The dark gray cells in Fig. 3 represent the neighbor data which will be averaged to estimate the noise parameters. These cells are called *reference cells* (N). The lighter gray cells in Fig. 3, immediately next to the cell under test, are called *guard cells* (G). These cells are excluded from the average.

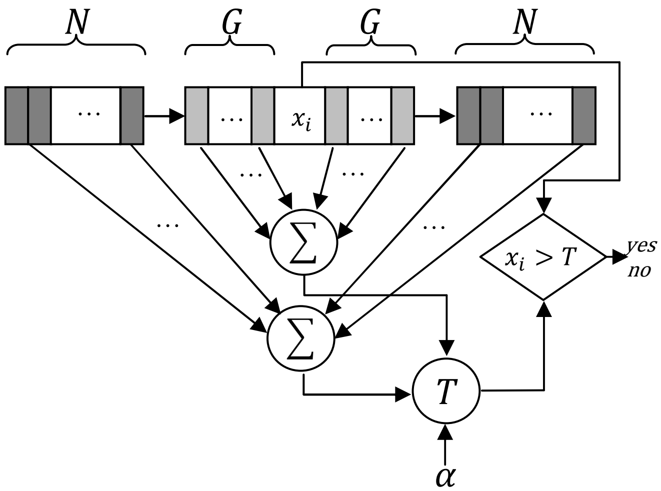

Figure 3: Generic architecture of the process CA-CFAR [39] y [40].

The reason for this exclusion is that if the objective is present; the neighbor cells contain similar values. In this case, the energy in the cells next to x_i should contain the same interference energy along with the objective, and should not be representative with its own interference. This extra energy that the objective contains should tend to increase the estimation of the interferences parameters. The total number of reference and guard cells utilized in each estimation is calculated utilizing the following equations, with $G < N$:

$$N_c = 2N + 1 \quad (2)$$

$$G_c = 2G + 1 \quad (3)$$

The procedure to determine the detection threshold (T) which we selected in this opportunity is described. Let us consider the case of a Gaussian interference with a quadratic rule detector. The *probability density function* (*pdf*), for any cell x_i, it has only one free parameter which is the media of the interference power(β^2). Likewise, the process estimates the media of the interference power in the test cell using the adjacent cells data. It is supposed that their interference is *independent and identically distributed (i.i.d)*, for a media of the total interference power β^2, it is:

$$p_{x_i}(x_i) = \frac{1}{\beta^2}\, e^{-x_i/\beta^2} \quad (4)$$

It is supposed that N_c neighbor cells will be utilized, on the test cell, to estimate the interference power β^2. The union of the probability density function for a vector x of N_c samples is:

$$p_x(x) = \frac{1}{\beta^{2N_c}} \prod_{i=1}^{N_c} e^{-x_i/\beta^2} = \frac{1}{\beta^{2N_c}}\, e^{-(\sum_{i=1}^{N_c} x_i)/\beta^2} \quad (5)$$

The equation (5) is the probability function Λ for the vector of observed data $\boldsymbol{x}$. The maximum estimated probability of β^2 is obtained by maximizing with $\sum \boldsymbol{x_i}$ the equation (5) [38]. It is more convenient to maximize the function of the maximum probability logarithm [20]:

$$\ln \Lambda = -N_c \ln(\beta^2) - \frac{1}{\beta^2}\left(\sum_{i=1}^{N_c} x_i\right) \quad (6)$$

Deriving the equation (6) with respect to β^2 and equaling to 0 it is obtained:

$$\frac{d(\ln \Lambda)}{d(\beta^2)} = 0 = -N_c\left(\frac{1}{\beta^2}\right) - \left(-\frac{1}{(\beta^2)^2}\right)\left(\sum_{i=1}^{N_c} x_i\right) \quad (7)$$

Solving the equation (7) for β^2, the maximum estimated probability will be the average of the available samples:

$$\widehat{\beta^2} = \frac{1}{N_c}\sum_{i=1}^{N_c} x_i \quad (8)$$

The required threshold detection is estimated as a multiple of the interference power:

$$\hat{T} = \alpha\widehat{\beta^2} \quad (9)$$

The attempt to calculate an adaptive threshold is to provide a constant false alarm rate even though the interference power levels may vary. The computation of this threshold, according to equation (9), is represented as a random variable, as well as the probability of false alarm. The detector is considered CFAR if the value of P_{fa}, does not depend on the current value of β^2. Combining equations (8) and (9) the expression for the estimated threshold is a:

$$\hat{T} = \frac{\alpha}{N_c}\sum_{i=1}^{N_c} x_i \quad (10)$$

Defining

$$z_i = \left(\frac{\alpha}{N_c}\right) x_i$$

such that

$$\hat{T} = \sum_{i=1}^{N_c} z_i,$$

and using the standard result of the probability theory with equation (4) the *pdf* of z_i can be represented by:

$$p_{z_i}(z_i) = \frac{N_c}{\alpha\beta^2}\, e^{-N_c z_i/\alpha\beta^2} \quad (11)$$

The *fdp* of $\hat{T}$ is known as *Erlang density*:

$$p_{\hat{T}}(\hat{T}) = \left(\frac{N_c}{\alpha\beta^2}\right)^{N_c} \frac{\hat{T}^{N_c-1}}{(N_c-1)!} e^{-N_c\hat{T}/\alpha\beta^2} \quad (12)$$

The observed P_{fa} with the estimated threshold will be $exp(-\hat{T}/\beta^2)$, also a random variable whose expected value is calculated as:

$$\bar{P}_{fa} = \int_{-\infty}^{\infty} e^{-\frac{\hat{T}}{\beta^2}} p_{\hat{T}}(\hat{T}) d\hat{T}$$

$$\bar{P}_{fa} = \left(\frac{N_c}{\alpha\beta^2}\right)^{N_c} \frac{1}{(N_c-1)!} \int_{-\infty}^{\infty} \hat{T}^{N_c-1} e^{-\left|\left(\frac{N_c}{\alpha}\right)+1\right|\hat{T}/\beta^2} d\hat{T} \quad (13)$$

Completing the standard integral and carrying out some algebraic manipulation, the final resulted is obtained:

$$\bar{P}_{fa} = (1 + \frac{\alpha}{N_c})^{-N_c} \quad (14)$$

For an expected $\bar{P}_{fa}$, the required value of the threshold multiplier is acquired solving equation (14):

$$\alpha = N_c\left(\bar{P}_{fa}^{-\frac{1}{N_c}} - 1\right) \quad (15)$$

Note that $\bar{P}_{fa}$ does not depend on the interference power β^2, but on the number N_c of neighbor cells and the threshold multiplier α. Thus, the technique of cells average exhibits the CFAR behavior.

A. *CA-CFAR of partial sums*

The *CA-CFAR of partial sums* represent a variant in the implementation of the standard CA-CFAR described in the previous section, in which a continuous average of the cells values is carried out to compute the threshold (T). In each step, a window of reference and guard cells are taken, which will be averaged utilizing equation (8). Once this value is calculated, the threshold is estimated, and then the presence of an objective is checked.

To carry out this calculation it is necessary to define a window of N_c reference cells which will be slid over all the samples until the process is finished. Consequently, for each adaptive threshold-estimation for each sample to analyze, N_c accesses to memory are carried out for the calculation of the summation of reference cells and N_G new accesses to memory for the guard cells computation. These calculations generate great computational resources consumption and excessive time to on-line analyze the entire data sample. For this reason, the improvement proposal is focused in the computation of the summation of reference and guard cells. (See Fig. 3).

The next Fig. 4 shows an example of the samples distribution $(x_1, \ldots, x_n)$ and calculation of the summation $(\sum_1, \ldots, \sum_n)$ for reference cells with $N = 2$ $(N_c = 5)$. As it can be observed for the calculation of the summation $\sum_3$, of the test cell x_3, the samples are needed $x_1, \ldots, x_5$. Likewise, this sample x_3 is utilized for the calculation of the summations $\sum_1, \ldots, \sum_5$. Having into account this detail, each sample is taken beforehand and is used in $N_c = 5$ summations which need this value, generating its final value based on the partial additions of samples. This process is carried out before estimating the threshold and checking the detection. This tasks separation generates a great saving of computational resources and time.

The method is applied likewise to the calculation of the summation of the guard cells.

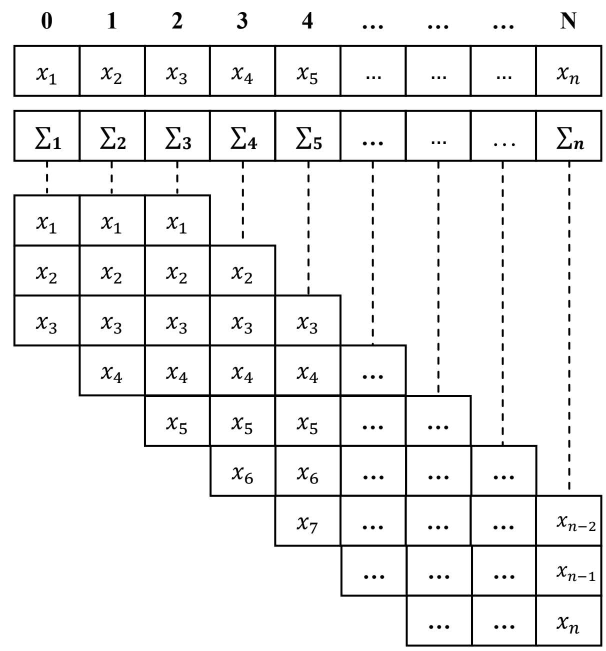

Figure 4: Distribution of the cells values for the technique CA-CFAR of partial sums $(N = 2, N_c = 5)$.

V. Experimental Results

The algorithms were developed originally with MATLAB even though later were ported to C++ code, taking advantage from the data structure of OpenCV. The algorithms were executed on a PC with a CPU 2-GHz Intel(R) Core(TM) 2 Duo, and 2-GB RAM memory. The SSS was the Tritech StarFish 450F, performing CHIRP techniques in the range of 430 to 470 KHz.

A. *Data from sea trials*

The test data for this work were acoustic images of the seafloor with the presence of a pipeline in Salvador de Bahía, Brazil. An important amount of 50500 lines of valid acoustic data were collected from the aforementioned SSS, which provided 101 images of 1000x500.

Fig. 5 shows a group of original acoustic images examples of the SSS (a), and the output after applying the processing chain (b). These images have been formatted for their best presentation. In all the cases the pipeline is on the right side. Fig. 5.1 and Fig. 5.4 show pipeline in a well-defined straight line.

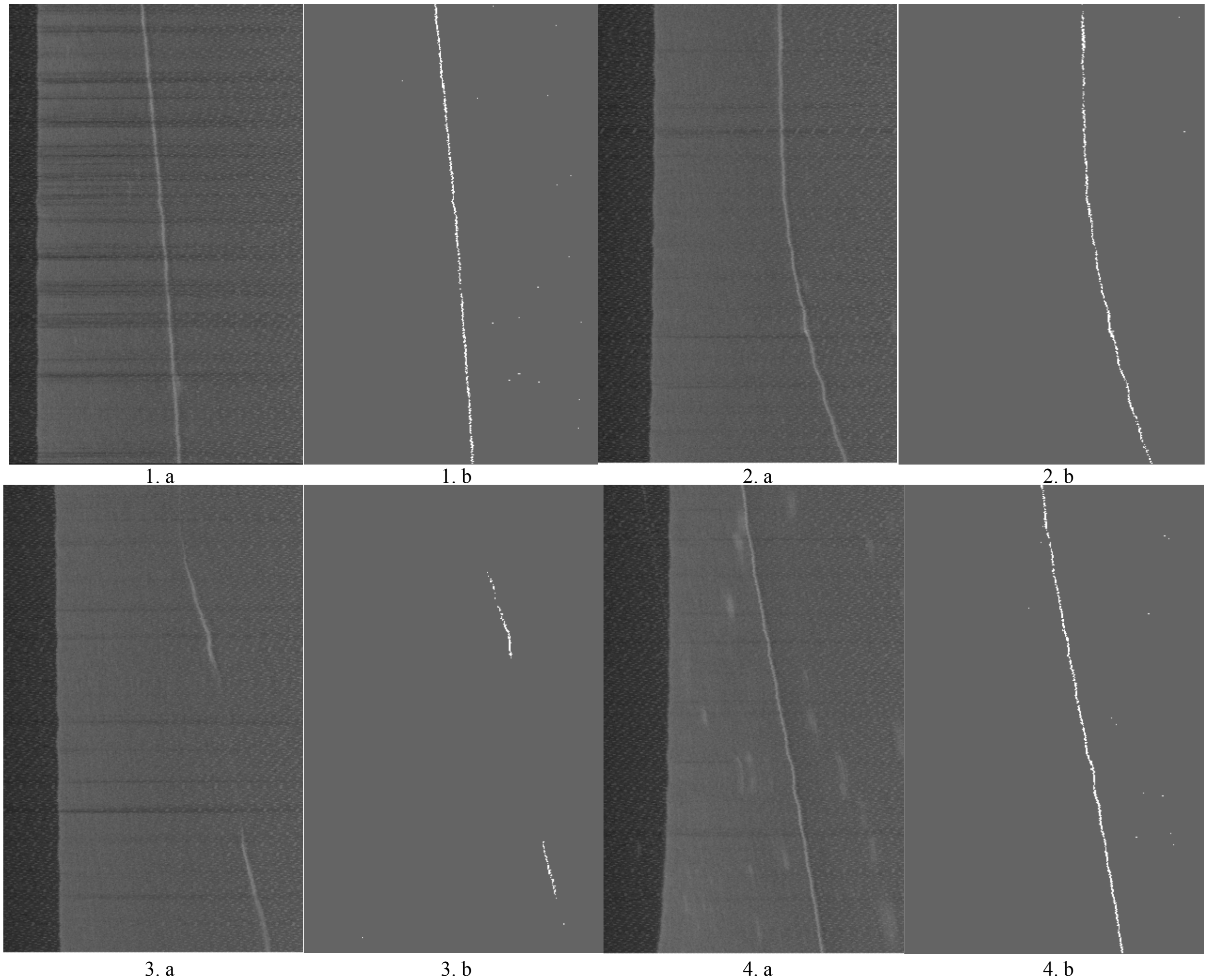

Figure 5: Results when applying the automatic processing chain: a) original, b) final result.

Instead, in Fig. 5.2 the pipeline forms a little curve. In Fig. 5.3 the pipeline is semi buried with sections on the surface. In all the cases it can be observed an efficient acoustic images treatment by mean of the proposed detection system.

B. *Comparison Measure*

Focusing in the comparisons of the two presented algorithms, two quantitative measures were utilized: the instructions quantity and the execution time in seconds. The first quantitative measure represents the number of necessary instructions for the algorithm execution. The equation (16) represents the instructions calculation for the standard CA-CFAR, where S_w and S_a represent acoustic lines quantity (*swath*) and the samples taken (*samples*), respectively.

Besides, N and G represent the reference and guard cells number, respectively.

$$\#\mathrm{I} = S_w * (S_a - 2 * (\mathrm{N} + \mathrm{G} + 1)) * (2 * (\mathrm{N} + \mathrm{G}) + 1) \quad (16)$$

The following equation (17) shows the calculation of the number of algorithmic instructions for the technique CA-CFAR of partial sums:

$$\#\mathrm{I} = \mathrm{S_w} * \mathrm{S_a} * (\mathrm{N} + \mathrm{G} + 1) \quad (17)$$

C. *Comparison between both approaches*

The Table I shows the values utilized for the automatic detection process with the technique CA-CFAR and its variant of partial sums. For each test cell, N_c and N_G neighbor cells are utilized (equation 2 and 3) to calculate adaptive threshold and determine the presence or absence of pipeline. The number of found detections is stored in a file with its respective geographic coordinate.

Both presented approaches show equal results but with a notable difference in the CPU instructions number. The improvement reduces more than 50% of necessary CPU instructions, which impacts on the execution time.

It should also must be taken into account that when the reference and guard cells number increase, the gap in the difference of the CPU instructions number in both algorithms also increase.

In the images the false detections are noted like white points without correlation in neighbor lines, which should be corrected by means of some post-processing or improvement in the detection method.

TABLE I
DATA AND RESULTS OF DETECTION TECHNIQUES

#	Téc.	N	G	α	P_{fa}	# D	# I	T (seg)
1	S	18	6	2,05	0,136	896	23275000	0,993
	SP						12500000	0,54
2	S	18	6	2,05	0,136	794	23275000	0,9
	SP						12500000	0,539
3	S	18	8	2,05	0,136	220	23275000	0,878
	SP						12500000	0,527
4	S	32	6	1,60	0,205	1113	35958000	1,03
	SP						19500000	0,753

Image 500x1000 (500000 samples). S: CA-CFAR standard technique, SP: CA-CFAR of partial sums technique. N: reference cells. G: guard cells. # D: number of detections. # I: number of instructions (equation 16 and 17).

VI. Conclusions

In this work, it was presented an automatic processing chain for a pipeline detection system from acoustic data obtained from a moving vehicle, utilizing a cell averaging technique with constant false alarms rate. Also, a variant CA-CFAR of partials sums was presented which provides equal results in much less time due to computational resources savings. The technique CA-CFAR has its origin in the radar signals processing. In this work it was also proved the benefit of migrating this technique for the objectives detection in acoustic images of SSS. As the final objective was to employ this automatic detection system on board of an ASV or AUV, an increase of efficiency in processing techniques was essential. This approach seems to be very promising in this sense and will be included for wet trials with the AUV ICTIOBOT prototype [41] altogether with its dynamic mission planning, guidance and control systems.

VII. Acknowledgements

This work was carried out thanks to the following projects financing: DPI2009-11298, MICINN from Spain, CONICET – PIP 11420090100238, and ANPCyT – PICT-2009-0142 from Argentina. Author Sebastian Villar wants to acknowledge the IEEE/OES Student Scholarships with which he was granted for his postgraduate studies.

References

[1] A. Balasuriya and T. Ura, “Multi-sensor fusion for autonomous underwater cable tracking,” in *OCEANS’99 MTS/IEEE*, vol. 1, pp. 209-215, September 1999.

[2] A. Ishøy, A. Bjerrum, O. Calvo, G. G. Acosta, Y. Petillot, J. Evans, K. Kyruakopoulos, G. Lionis, T. Slater and R. Nunn, “New challenges for AUTOTRACKER,” *Unmanned Underwater Vehicle Showcase (UUVS, 02)*, Southampton, UK, September 2002.

[3] X. Lurton, *An introduction to Underwater Acoustics*, Ed. Springer Verlag Inc. 2003.

[4] P. Chapple, “Automated Detection and Classification in High-resolution Sonar Imagery for Autonomous Underwater Vehicle Operations,” *Maritime Operations Division. DSTO Defence Science and Technology Organisation*, 2008.

[5] G. G. Acosta, H. Curti and O. Calvo, “Autonomous underwater pipeline inspection in AUTOTRACKER PROJECT: the Navigation Module,” in *IEEE/OCEANS’05 Europe Conference*, vol. 1, pp. 389-394, June, 2005.

[6] M. Mignotte, C. Collet, P. Perez, and P. Bouthemy, “Three-class Markovian segmentation of high-resolution sonar images,” in *Computer Vision and Image Understand*, vol. 76, issue 3, pp. 191–204, 1999.

[7] M. Mignotte, C. Collet, P. Perez, and P. Bouthemy, “Sonar image segmentation using an unsupervised hierarchical MRF model,” in *IEEE Transactions Image Process.*, vol. 9, issue 7, pp. 1216–1231, July, 2000.

[8] T. F. Chan, B. Y. Sandberg and L. A. Vese, “Active contours without edges for vector-valued images,” in *Journal of Visual Communication and Image Representation,* vol. 11, issue 2, pp. 130–141, June, 2000.

[9] R. C. González and R. E. Woods, *Digital Image Processing Second Edition*, Prentice Hall Upper Saddle River, New Jersey 07458, 2001. ISBN 0-201-18075-8.

[10] W. K. Pratt, *Digital Image Processing: PIKS Inside*, 3er ed., 2001. ISBN: 0-471-37407-5

[11] F. Zhou, J. F. Feng, and Q. Y. Shi, “Texture feature based on local Fourier transform,” in *International Conference on Image Processing*, vol. 2, pp. 610–613, October, 2001.

[12] G. R. Cutter, Y. Rzhanov, and L. A. Mayer, “Automated segmentation of seafloor bathymetry from multibeam echosounder data using local Fourier histogram texture features,” in *Journal Experimental Marine Biology and Ecology,* vol. 285–286, pp. 355–370, February 2003.

[13] S. Reed, I. T. Ruiz, C. Capus, and Y. Petillot, “The fusion of large scale classified side-scan sonar image mosaics,” in *IEEE Transactions Image Process*, vol. 15, issue 7, pp. 2049–2060, July, 2006.

[14] M. Lianantonakis and Y. Petillot, “Sidescan sonar segmentation using texture descriptors and active contours,” in *IEEE Journal Oceanic Engineering*, vol. 32, issue 3, pp. 744–752, July, 2007.

[15] I. Karoui, R. Fablet, J. M. Boucher, and J. M. Augustin, “Seabed segmentation using optimized statistics of sonar textures,” in *IEEE Transactions Geoscience and Remote Sensing*, vol. 47, issue 6, pp. 1621–1631, June, 2009.

[16] D. Williams, “Bayesian data fusion of multiview synthetic apertura sonar imagery for seabed classification,” in *IEEE Transactions Image Process.,* vol. 18, issue 6, pp. 1239–1254, 2009.

[17] X. F. Ye, Z. H. Zhang, P. X. Liu, and H. L. Guan, “Sonar image segmentation based on GMRF and level-set models,” in *Oceanic Engineering*, vol. 37, issue 10, pp. 891–901, July, 2010.

[18] T. Celik and T. Tjahjadi, “A Novel Method for Sidescan Sonar Image Segmentation,” in *IEEE Journal of Oceanic Engineering*, vol. 36, issue 2, pp. 186 –194, April, 2011.

[19] D. K. Barton and S. A. Leonov, *Radar Technology Encyclopedia,* Artech House, 1998. ISBN 0-89006-893-3.

[20] M. A. Richards, *Fundamental of radar signals processing*, Mc Grae Hill Electronic Engineering. Georgia institute of technology, 2005. ISBN-0-07-144474-2.

[21] R. E. Hansen, “Introduction to sonar,” *Course materiel to INF-GEO4310*, University of Oslo, 2009.
[22] Y. Petillot, S. Reed and J. Bell, “Real time AUV pipeline detection and tracking using side scan sonar and multi-beam echo-sounder,” in *Oceans 2002 MTS/IEEE*, vol. 1, issue 29-31, pp. 217–222, October, 2002.
[23] S. Reed, Y. Petillot and J. Bell, “A Model Based Approach to Mine Detection and Classification in Sidescan Sonar,” in *Oceans 2003,* vol. 3, issue 22-26, pp. 1402-1407, September, 2003.
[24] S. Reed, Y. Petillot and J. Bell, “An automatic approach to the detection and extraction of mine features in sidescan sonar,” in *IEEE Journal Oceanic Engineering*. vol. 28, Issue 1, pp. 90-105, January, 2003.
[25] S. Reed, Y. Petillot and J. Bell, “Automated approach to classification of mine-like objects in sidescan sonar using highlight and shadow information,” in *IEEE Processing Radar, Sonar & Navigation 151* (No.1), pp. 48-56, February, 2004.
[26] S. W. Perry and L. Guan, “A Recurrent Neural Network for Detecting Objects in Sequences of Sector-Scan Sonar Images,” in *IEEE Journal of oceanic engineering*, vol. 29, issue 3, pp. 857-871, July, 2004.
[27] J. M. Bell, Y. R. Petillot, K. Lebart, P. Y. Mignotte and H. Rohou, “Target recognition in synthetic aperture and high resolution sidescan sonar,” *IET Seminar on High Resolution Imaging and Target Classification*, London, UK, pp. 99-106, November, 2006.
[28] R. E. Hansen, J. Groen and H. J. Callow, “Image enhancement in synthetic aperture sonar,” in *Detection & Classification of Underwater Targets,* Institute Acoustics 29, Part 6, pp. 69-76, 2007.
[29] T. O. Sæbø, H. J. Callen and R. E. Hansen, “Bathymetric capabilities of the HISAS interferometric synthetic aperture sonar,” in *MTS/IEEE Oceans 2007*, pp. 1-10, September, 2007.
[30] T. Sparr, R. E. Hansen, H. J. Callow and J. Groen, “Enhancing target shadows in SAR images,” in *Electronics Letters,* vol. 43, Issue 5, pp. 69-70, March, 2007.
[31] P. E. Hagen and R. E. Hansen, “Synthetic aperture sonar challenges,” in *Hydro International,* vol. 12, issue 4, pp. 26-31, May 2008.
[32] A. M. Pavin, “The Pipeline Identification Method Basing on AUV's Echo-Sounder Data,” in *Oceans 2006,* pp. 1-6, September, 2006.
[33] B. Jalving, M. Mandt, O. Hagen, and F. Pøhner, “Terrain referenced navigation of AUVs and submarines using multibeam echo sounders,” in *UDT Europe 2004*, Nice, France, 2004.
[34] S. F. Greenaway and T. C. Weber, “Test methodology for evaluation of linearity of multibeam echosounder backscatter performance,” in *Oceans 2010,* pp. 1-7, September, 2010.
[35] P. S. Chavez, Jr, “Processing techniques for digital sonar images from GLORIA,” in *Photogeometric Eng. Remote Sens.*, vol. 52, pp. B, 1976.
[36] A. R. Stubbs, “Identification of patterns of asdic records,” in *International Hydrographic. Review*, vol. 40, pp. 53-68, 1963.
[37] D. T. Cobra, “Estimation and correction of geometric distortions in side-scan sonar images,” *Ph.D. dissertation, Mass. Inst. Of Technology and Woods Hole Ocean. Inst*, 1990.
[38] S. M. Kay, *Fundamentals of Statistical Signal Processing*, vol. I: Estimation Theory. Prentice Hall, Upper Saddle River, NJ, 1993.
[39] M. I. Skolnik, *Introduction to Radar Systems.* McGraw-Hill; 2nd ed., 1980.
[40] M. I. Skolnik, *Radar Handbook*. McGraw-Hill; 2nd ed., 1990.
[41] G. G. Acosta, H. Curti, O. Calvo Ibáñez, and S. Rossi, *Some Issues on the Design of a Low-Cost Autonomous Underwater Vehicle with an Intelligent Dynamic Mission Planner for Pipeline and Cable Tracking*, , Chapter I in Underwater Vehicles, pp. 1-18 I-Tech Online Books, Robotics Series, I-Tech Education and Publishing KG, Viena, Austria, 2009, <Open Access: http://books.i-techonline.com/> . (ISBN 978-953-7619-49-7)